Muonium centers in the cuprous halides

R. F. Kiefl,* W. Odermatt, Hp. Baumeler, J. Felber, H. Keller, W. Kündig,
P. F. Meier, B. D. Patterson, and J. W. Schneider
Physics Institute, University of Zurich, 8001, Zurich, Switzerland

K. W. Blazey
IBM Research Laboratory, 8803 Rüshlikon, Switzerland

T. L. Estle
Physics Department, Rice University, Houston, Texas 77251

C. Schwab
Laboratoire de Spectroscopie et d'Optique du Corps Solides, Université Louis Pasteur, 67000 Strasbourg, France
(Received 4 March 1986)

Muon-spin-rotation measurements in the group I-VII semiconductors CuCl, CuBr, and CuI reveal muonium centers with weak isotropic hyperfine (hf) parameters which range between 0.2716 and 0.3744 times the hf parameter for muonium in vacuum. The observed centers display several unusual characteristics when compared with muonium in other tetrahedrally coordinated materials. In particular the hf parameters in the copper halides are much smaller than expected on the basis of their ionicity. Also, in CuCl and CuBr two distinct muonium centers (Mu^{I} and Mu^{II}) with almost identical isotropic hf parameters are observed for the first time. The Mu^{I} center is populated preferentially at low temperature but makes a thermally activated transition to Mu^{II}, indicating that Mu^{I} is less stable than Mu^{II}. Measurements of the line broadening in the magnetic field region 0.2–1.2 T indicate that there is no motional averaging of the nuclear hyperfine interaction and therefore that the centers are close to being static.

I. INTRODUCTION

An energetic positive muon (μ^+) which is implanted into a semiconductor or insulator may end up in a variety of different locations and charge states in the crystal. Those centers which are paramagnetic are termed muonium defect centers since, as in the hydrogenlike atom muonium (μ^+e^-), there is a hyperfine (hf) interaction between the muon and the unpaired electron. Muonium defect centers provide a unique opportunity to compare the electronic structure of a simple defect in a unprecedented range of materials which now include elemental semiconductors,[1,2] solid noble gases,[3] molecular solids,[4,5] and very recently, ionic insulators[6] and group–III-V compound semiconductors.[7] Furthermore, the technique of muon-spin rotation (μSR) allows one to observe directly dynamical processes involving muonium which occur within the lifetime of the positive muon in the sample (2.2 μs). Unlike the EPR of hydrogen, the technique of μSR is perfectly selective since only centers involving the muon are observed. Also, the number of implanted muons is typically less than 10^9 per sample and, consequently, the radiation damage caused by the muons is negligible.

Muonium in semiconductors is of special interest since there have been no EPR measurements of hydrogen in a semiconductor. Over the past ten years a large body of information on muonium defect centers in the group-IV elemental semiconductors has become available.[1,2] Two types of muonium centers, "normal" muonium (Mu) and anomalous muonium (Mu^*), have been observed in Si, Ge, and diamond. Mu is characterized by a large isotropic hf interaction about half that of muonium in vacuum, whereas Mu^* has a relatively small and anisotropic hf interaction with $\langle 111 \rangle$ symmetry. Several theoretical studies[8–11] indicate that Mu is a neutral atom which has a minimum potential energy at the tetrahedral interstitial site but with only a small barrier between equivalent sites. Experimental work confirms that Mu is moving rapidly in the elemental semiconductors.[12] There has been considerable debate on the site of Mu^*. Recent theoretical work[13–15] indicates that Mu^* is located at a vacancy rather than at the hexagonal interstitial site as proposed earlier.[16] However, there are still difficulties in explaining the formation of a muon-vacancy complex.[7]

There are numerous reasons for extending the study of muonium defect centers to compound semiconductors. For example, the effect of covalency of the host on the electronic structure of the muonium centers can be investigated by comparing results in the group–IV, group–III-V, group–II-VI, and group–I-VII materials with the same crystal structure. Also, the group–III-V and group–I-VII compounds contain a high percentage of nuclear moments and thus provide an opportunity to study nuclear hyperfine (nhf) structure. Unlike the isotropic hf structure of normal muonium, the nhf structure is sensitive to diffusion. In addition, measurements of the nhf parameters would provide important new information on the electron-spin-density distribution away from the muon.

Recently, in the group–III-V compound semiconduc-

tors GaAs and GaP, we have observed muonium centers[7] which resemble the Mu and Mu* centers seen previously in Si, Ge, and diamond. All muonium parameters in GaAs are remarkably similar to those in GaP, indicating that sites with Ga nearest neighbors are occupied preferentially.

In this paper we report detailed measurements on the electronic structure of muonium defect centers in the group—I-VII compound semiconductors CuCl, CuBr, and CuI. These are the most ionic of all the tetrahedrally coordinated materials and in this sense lie between the pure covalent group-IV semiconductors and the highly ionic group—I-VII insulators, the alkali halides. The results are surprising in two ways. First, the hf parameters for muonium in CuCl, CuBr, and CuI range between 0.2716 and 0.3744 times the hf parameter for muonium in vacuum. This is considerably smaller than for normal muonium in ionic crystals[6] or covalent semiconductors.[1,2,7] Second, in CuCl and CuBr two distinct muonium centers with almost identical isotropic hf parameters are seen for the first time. One center, which we call Mu^{I}, is populated preferentially at low temperatures, but makes a thermally activated transition to a second center, Mu^{II}.

II. THEORY

A. The spin Hamiltonian

When the muonium defect center is localized about a site with high symmetry the spin Hamiltonian is of the following form:

$$\mathcal{H}/h = A\mathbf{S}\cdot\mathbf{I}+\gamma_e\mathbf{S}\cdot\mathbf{B}-\gamma_\mu\mathbf{I}\cdot\mathbf{B} + \sum_n(\mathbf{S}\cdot\overleftrightarrow{C}^n\cdot\mathbf{J}^n+\mathbf{J}^n\cdot\overleftrightarrow{Q}^n\cdot\mathbf{J}^n-\gamma_n\mathbf{J}^n\cdot\mathbf{B}) , \quad (1)$$

where $\mathbf{S}$, $\mathbf{I}$, and $\mathbf{J}^n$ are the electron, muon, and nth neighboring nuclear spin, A is the isotropic muon hf parameter, $\overleftrightarrow{C}^n$ is the nhf tensor, $\overleftrightarrow{Q}^n$ is the nuclear electric quadrupole (neq) tensor, and $\mathbf{B}$ is the magnetic field. The g tensors, contained within the gyromagnetic ratios ($\gamma_i=g_i\mu_i/h$), are all taken to be positive and isotropic. A more general form for $\mathcal{H}$ may be obtained by allowing the electron Zeeman and muon hf interactions to be anisotropic.[17] This would be necessary if the muonium defect center were in a site with lower symmetry.

B. Frequency spectrum in the absence of nuclear hyperfine interaction

In the absence of nhf interaction the time evolution of the muon polarization is determined by the first three terms in Eq. (1), which are of the same form as for muonium in vacuum. If the electron is unpolarized and a high magnetic field is applied transverse to the initial muon polarization, then two muon precession frequencies of equal amplitude are expected:

$$\nu_1=\tfrac{1}{2}A[1+(\Gamma_-/\Gamma_+)x-(1+x^2)^{1/2}] , \quad (2a)$$

$$\nu_2=-\tfrac{1}{2}A[1-(\Gamma_-/\Gamma_+)x+(1+x^2)^{1/2}] , \quad (2b)$$

where $\Gamma_\pm=(\gamma_e\pm\gamma_\mu)/2$, $x=B/B_0$, and B_0 is the hf field, equal to $A/2\Gamma_+$. In the high-field region ν_1 and ν_2 correspond to $\Delta I_z=\pm1$ transitions, for which $S_z=+\frac{1}{2}$ and $S_z=-\frac{1}{2}$, respectively. Note that the sense of precession of frequency ν_2 is opposite to that of ν_1 except in the extreme high-field limit, $x\gtrsim m_\mu/2m_e\simeq103$. The field dependence of these frequencies is shown in Fig. 1. At the special field corresponding to

$$x_M=[(\Gamma_+/\Gamma_-)^2-1]^{-1/2} , \quad (3)$$

the muonium frequencies have a broad maximum and minimum, respectively. Thus, near x_M or above the frequencies are much less sensitive to field inhomogeneity than in the low-field region. The hf parameter and ratio between the electron and muon g factors can be expressed in terms of ν_1, ν_2, and the Larmor precession frequency of the muon, ν_μ,

$$A=\nu_1-\nu_2 , \quad (4a)$$

$$\frac{g_e}{g_\mu}=\frac{m_e}{m_\mu}\frac{2\nu_1\nu_2+(\nu_1+\nu_2)\nu_\mu}{\nu_\mu(\nu_1+\nu_2+2\nu_\mu)} . \quad (4b)$$

For muonium in vacuum

$$\begin{aligned} &A=4463.302\ \text{MHz} ,\\ &g_e=2(1.001\,141\,9) ,\\ &g_\mu=2(1.001\,148\,1) ,\\ &\nu_\mu=135.5537\times B\ \text{MHz/T} ,\\ &\Gamma_+=14\,079.87\ \text{MHz/T} ,\\ &\Gamma_-=13\,944.34\ \text{MHz/T} , \end{aligned} \quad (4c)$$

where the g factors include relativistic bound-state corrections to the free-particle values.[18]

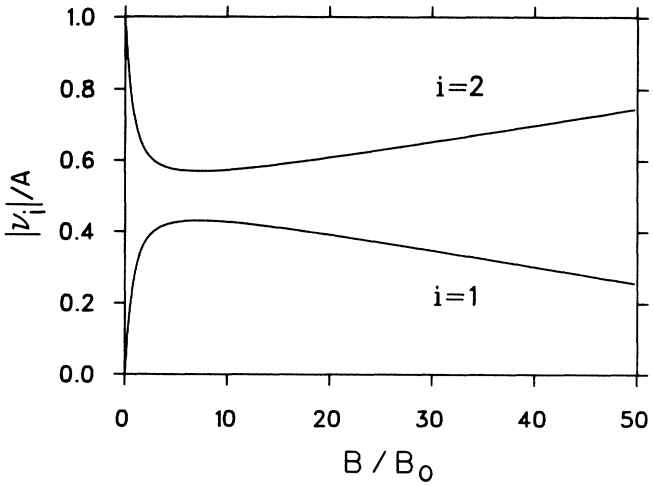

FIG. 1. The absolute value of the two dominant precession frequencies for vacuumlike muonium in a high transverse magnetic field. The sign of ν_2 is opposite to that of ν_1 in this field region. The magnetic field and frequencies are in units of the hyperfine field B_0 and hyperfine parameter A, which for muonium in vacuum are equal to 0.1585 T and 4463.302 MHz, respectively.

C. Line broadening due to nuclear hyperfine interaction

Inclusion of the nhf terms in Eq. (1) leads to a complicated frequency spectrum in low transverse fields consisting of many small-amplitude lines which cannot be resolved. However, in high transverse magnetic fields where the muon, electron, and nuclear spins are essentially decoupled, the frequency spectrum reduces to the simple two-component spectrum observed in the absence of nhf interaction.[19,6] In the intermediate-field region the nhf interaction produces small splittings in the primary lines which appear in our spectra as a line broadening. For the purpose of calculating this line broadening, we consider a model spin system consisting of a muon, an electron, and N identical nuclei with spin $\mathbf{J}^n$. We assume that the nhf interaction is isotropic and neglect the effects of neq interaction. The resulting spin Hamiltonian is then

$$\mathscr{H}/h = A\mathbf{S}\cdot\mathbf{I}+\gamma_e\mathbf{S}\cdot\mathbf{B}-\gamma_\mu\mathbf{I}\cdot\mathbf{B}+C\mathbf{S}\cdot\mathbf{J}-\gamma_n\mathbf{J}\cdot\mathbf{B}\ , \tag{5}$$

where $\mathbf{J}$ is the total nuclear spin and C is the isotropic nhf parameter. Roduner and Fischer[19] have treated a similar problem in regard to muonated free radicals. Provided that $\gamma_e B \gg A \gg C$, and there are no accidental degeneracies, then an approximate muon-spin frequency distribution in high transverse fields may be obtained from nondegenerate perturbation theory, treating the nhf interaction as a perturbation. The first-order splittings in the precession frequencies are proportional to the component of $\mathbf{J}$ along the magnetic field direction, $\hat{\mathbf{z}}$:

$$\nu_1(J_z)=\nu_1(0)+CJ_z\sin^2\theta\ , \tag{6a}$$

$$\nu_2(J_z)=\nu_2(0)+CJ_z\sin^2\theta\ , \tag{6b}$$

where

$$\sin^2\theta=\tfrac{1}{2}[1-x/(1+x^2)^{1/2}]$$
$$\simeq 1/4x^2 \text{ for large } x\ , \tag{6c}$$

and $\nu_1(0)$ and $\nu_2(0)$ are the precession frequencies in the absence of nhf interaction given by Eqs. (2a) and (2b). Thus the nhf interaction causes frequencies ν_1 and ν_2 to split into $2NJ^n+1$ frequencies which are weighted by the probability of finding the N nuclear spins with total $\hat{\mathbf{z}}$ component of spin, J_z. Assuming there is no nuclear polarization, the resulting discrete frequency distribution lies within an approximately Gaussian envelope. The number of frequencies increases rapidly if one includes second-order corrections, the anisotropy of the nhf interaction, the presence of next-nearest neighbors, and the neq interaction. However, present techniques do not permit us to resolve the nhf structure and so we are only interested in calculating a linewidth parameter, which should be relatively insensitive to these latter effects. We define a Gaussian linewidth parameter,

$$\sigma(x)\equiv\pi(2M_2)^{1/2}=\Delta\sin^2\theta\ , \tag{7a}$$

where M_2 is the second moment of the frequency distribution and

$$\Delta=C\pi\left[2\sum_{J_z}m(J_z)J_z^2\right]^{1/2}. \tag{7b}$$

The multiplicity factor $m(J_z)$ is the random probability of finding the N nuclear spins with a total $\hat{\mathbf{z}}$ component of nuclear spin J_z. It is clear from Eq. (7a) that field dependence of σ can be used to determine the parameter Δ, which may be interpreted as the overall strength of the nhf interaction. If the number of nearest neighbors and their spins are known, then an approximate nhf parameter can be determined from Δ.

Until now we have implicitly assumed that the muonium center is static in the crystal. If the center is diffusing at a rate fast compared to the static linewidth, then the frequency lines will be motionally narrowed. Fast hopping results in a Lorentzian line shape with a width parameter λ given by

$$\lambda=2\sigma^2\tau_c=2\Delta^2\sin^4\theta\tau_c\ , \tag{8}$$

where τ_c is the mean time between hops. This expression is valid provided $\sigma\tau_c \ll 1$. Note that λ varies as $1/x^4$ in the high-field limit, whereas σ varies as $1/x^2$. Thus from the field dependence of the linewidth (or depolarization rate) we can determine if the muonium center is diffusing slowly or rapidly with respect to the static linewidth. This is considerably more sensitive to rapid diffusion than the line shape itself.

D. Transition between muonium states

Percival and Fischer[20] and Meier[21] have developed general theories to calculate the time evolution of the muon polarization when a transition occurs between muonium states with different hf parameters. If it is assumed that electron and muon spins are conserved at the instant of transformation, then in the limit of high transverse magnetic fields $x \gg 1$ the expectation value of the complex muon polarization, $p_\mu(t)=p_{\hat{\mathbf{x}}}(t)+ip_{\hat{\mathbf{y}}}(t)$, reduces to

$$p_\mu(t)=\tfrac{1}{2}\sum_{j=1}^{2}(\exp[(-\Lambda-i\omega_j^{\mathrm{I}})t]+\{1-\exp[-\Lambda-i(\omega_j^{\mathrm{I}}-\omega_j^{\mathrm{II}})t]\}\exp(-i\omega_j^{\mathrm{II}}t)/[1+i(\omega_j^{\mathrm{I}}-\omega_j^{\mathrm{II}})/\Lambda])\ , \tag{9}$$

where $\nu_j^{\mathrm{I}}=\omega_j^{\mathrm{I}}/2\pi$ and $\nu_j^{\mathrm{II}}=\omega_j^{\mathrm{II}}/2\pi$ are the high-field transition frequencies for the initial and final states, which we call Mu^{I} and $\mathrm{Mu}^{\mathrm{II}}$, respectively. When the transition rate Λ is small compared to $\omega_j^{\mathrm{I}}-\omega_j^{\mathrm{II}}$, the first term in bold parentheses dominates, corresponding to the initial-state frequencies, and the final-state frequencies corresponding to the second term are not observable. Note that the amplitudes for the initial state decrease exponentially in time at a rate Λ. On the other hand, if Λ is comparable to or larger than $\omega_j^{\mathrm{I}}-\omega_j^{\mathrm{II}}$ and provided $\Lambda t \gg 1$, then the second term dominates corresponding to the final state. The amplitudes a_j' and initial phases ϕ_j' associated with the final-

state frequencies are given by

$$2a_j' = \cos\phi_j' = \{1+[(\omega_j^{\mathrm{I}}-\omega_j^{\mathrm{II}})/\Lambda]^2\}^{-1/2}, \quad (10a)$$

$$\tan\phi_j' = (\omega_j^{\mathrm{II}}-\omega_j^{\mathrm{I}})/\Lambda . \quad (10b)$$

If there is a fraction of the muonium atoms f_p^{II} which form $\mathrm{Mu}^{\mathrm{II}}$ promptly in addition to the slow fraction f_s^{II} which begins as Mu^{I}, then the amplitudes and phases of the final state are given by

$$2a_j = [(f_p^{\mathrm{II}})^2 + 2f_s^{\mathrm{II}}f_p^{\mathrm{II}}\cos^2\phi_j' + (f_s^{\mathrm{II}})^2\cos^2\phi_j']^{1/2}, \quad (11a)$$

$$\tan\phi_j = \frac{f_s^{\mathrm{II}}\cos\phi_j'\sin\phi_j'}{f_p^{\mathrm{II}}+f_s^{\mathrm{II}}\cos^2\phi_j'} . \quad (11b)$$

If the transition rate from Mu^{I} to $\mathrm{Mu}^{\mathrm{II}}$ is temperature dependent, then the amplitude of $\mathrm{Mu}^{\mathrm{II}}$ and depolarization rate of Mu^{I} signal should also be temperature dependent. For example, if Λ has an Arrhenius behavior,

$$\Lambda(T) = \Lambda(\infty)\exp(-E_a/k_B t), \quad (12)$$

one expects that the Mu^{I} signal will disappear at a rate $\Lambda(T)$ and that the total amplitude of the $\mathrm{Mu}^{\mathrm{II}}$ signal will rise monotonically from f_p^{II} to $f_p^{\mathrm{II}}+f_s^{\mathrm{II}}$. The phases ϕ_j are also temperature dependent but are difficult to measure accurately because the muonium precession frequencies are large.

III. EXPERIMENTAL DETAILS

Single crystals of CuCl, CuBr, and CuI were cut from rods grown previously from the melt by one of us (C.S.), using a traveling-heater technique with $BaCl_2$, KBr, and KI as the respective fluxes.[22] The dimensions of the crystals were approximately 12 mm in diameter by 12 mm thick. The crystals were oriented in the case of CuCl and CuBr but not in the case of CuI. The overall contamination level has been estimated to be <100 ppm. The samples were cooled with a He-gas-flow cryostat and temperature measurements were made with a carbon resistor below 50 K and a platinum resistor above 50 K.

A diagram of the high-field (1.2 T) high-timing resolution μSR apparatus is shown in Fig. 2. The incoming beam of polarized positive muons from the μE4 beamline at the Swiss Institute for Nuclear Research are collimated down to a diameter of 10 mm before detection by the M_t counter. The incoming muons stop in the target crystal at an average rate of 10^5/s. The positrons from muon decay are detected by the E_t counter. A compact iron-core electromagnet (25-mm gap) is used to apply a magnetic field (0—1.2 T) transverse to the initial muon polarization. The design of this magnet is crucial in achieving the timing resolution necessary to resolve high-field muonium frequencies, which can be in excess of 2500 MHz for muonium defect centers with vacuum-like hf parameters. Note that the iron return yoke completely surrounds the magnet poles except for small entry ports for the muon beam, incoming muon counter M_t, the muon decay positron counter E_t, and the cryostat. With this design and μ-metal shielding the stray fields are reduced to 10 μT at a distance of only 10 cm from the magnet center. This permits the use of relatively short light guides between the

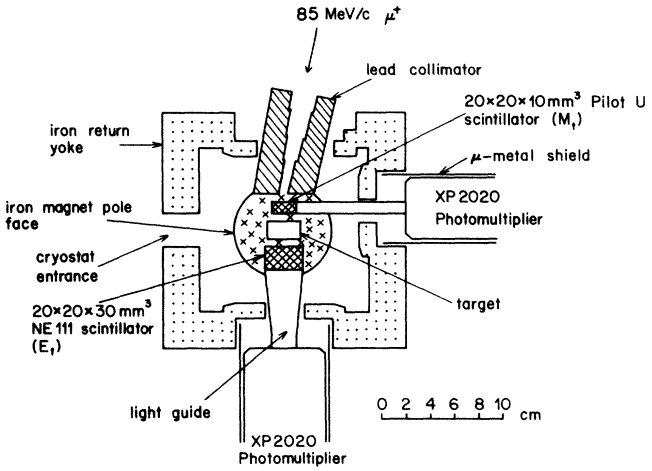

FIG. 2. The high timing resolution (205 ps) apparatus is used to resolve muonium precession frequencies in a large (1.2 T) transverse magnetic field. The return yoke of the compact iron-core electromagnet serves to contain the stray magnetic field and thus permits the use of short light guides between the fast plastic scintillators and photomultipliers.

plastic scintillators and photomultipliers which cannot operate in magnetic fields in excess of a 100 μT. The short light guides minimize the spread in transit times between the scintillator and photomultiplier, which is essential in achieving good timing resolution with this method of charged-particle detection. A significant (15%) improvement in the timing resolution was obtained by using quartz light guides instead of normal Plexiglass, since its transmission in the near-uv region allows a better matching to the light output spectrum from a NE111 scintillator obtained from Nuclear Enterprises Limited, Scotland. The frequency spectrum for muonium in high transverse magnetic fields provides a convenient measure of the timing resolution. In the high-field region where the muon and electron are decoupled, the two muonium frequencies [see Eqs. (2a) and (2b)] should have equal precession amplitude. However, the amplitude of the higher frequency is observed to be smaller than the amplitude of the lower frequency due to the finite timing resolution of the particle detection system. If one assumes a Gaussian resolution function, then using Eq. (7) of Ref. 23 the full width at half maximum δ may be expressed

$$\delta = \frac{2}{\pi}[\ln 2 \ln(a_1/a_2)/(\nu_2^2-\nu_1^2)]^{1/2}, \quad (13)$$

where a_1 and a_2 are the amplitudes of frequencies ν_1 and ν_2, respectively. The ratio a_2/a_1 was measured to be 0.656(37) in single-crystal SiO_2 at 305 K in a field of 1.15 T where $\nu_1 = 1936$ MHz and $\nu_2 = 2559$ MHz. This implies that the timing resolution of the detector system is 205(13) ps.

The general form of the μSR spectrum consists of an exponential decay modulated by the time evolution of the muon polarization. This modulation is a result of the asymmetric muon decay in which the decay positron is emitted preferentially along the muon-spin polarization direction. In a magnetic field transverse to the initial

muon polarization direction the lifetime spectrum takes the form

$$N(t)=N_0\exp(-t/\tau_\mu)[1+X(t)]+b\ , \tag{14a}$$

$$X(t)=\sum_{i=1}^{n} a_i R_i(t)\cos(2\pi\nu_i t+\phi_i)\ , \tag{14b}$$

where N_0 is a normalization, τ_μ is a muon lifetime (2.2 μs for positive muons), and b is a time-independent background. The parameters a_i, ν_i, and ϕ_i are the amplitudes, frequencies, and initial phases of the n different frequency components. The relaxation functions $R_i(t)$ are often assumed to be exponential,

$$R_i(t)=\exp(-\lambda_i t)\ , \tag{15a}$$

or Gaussian,

$$R_i(t)=\exp(-\sigma_i^2 t^2)\ , \tag{15b}$$

corresponding to a Lorentzian or Gaussian line shape, respectively. In the present analysis the complex Fourier transforms of the time spectra were fitted to the finite Fourier transform of Eq. (14b). In many instances the raw-time spectra were fitted directly to Eq. (14a) with no significant difference in results. Fits assuming Gaussian and exponential relaxation functions were compared in selected cases.

The time digitization was performed with a time-to-amplitude convertor (TAC) coupled to a 8192-channel analog-to-digital convertor (ADC). A high-resolution setting of 45 ps/channel was necessary to resolve the high frequencies expected in the experiment. This limited the length of the time spectra to 400 ns. The timescale was calibrated with a precession quartz calibrator. The errors on all precession frequencies include a small systematic uncertainty (less than 50 ppm) due to drifts in the time calibration. Typically, $(5-10)\times10^6$ events were collected in each spectrum with a good event rate of approximately 500/s.

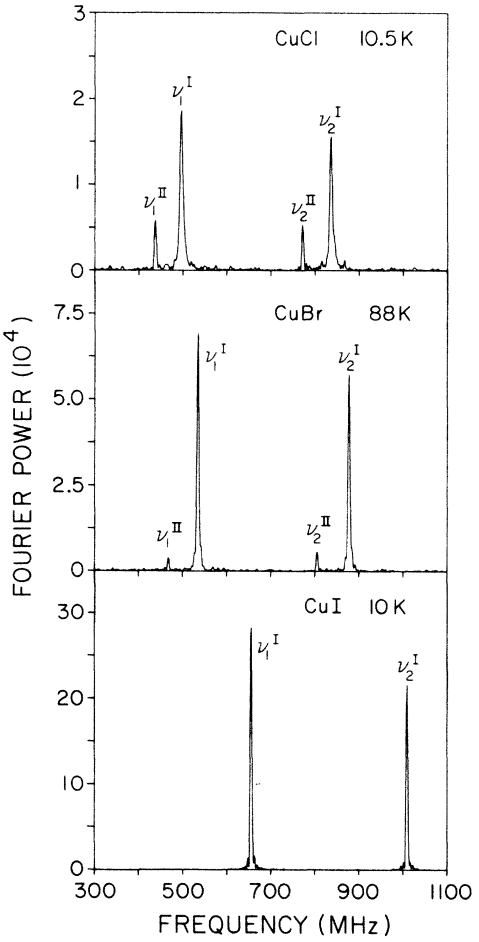

FIG. 3. The μSR frequency spectra in the Cu halides in a transverse magnetic field of 1.156 T. In CuCl and CuBr the two pairs of frequencies ν_i^I and ν_i^{II} are attributed to two distinct muonium centers (Mu^I and Mu^{II}) with isotropic hyperfine interactions.

IV. RESULTS

A. The muon hyperfine parameters for Mu^I and Mu^{II}

The muon-spin frequency spectra for CuCl, CuBr, and CuI in a high transverse magnetic field (1.2 T) are shown in Fig. 3. In CuCl and CuBr two pairs of frequencies (ν_i^I and ν_i^{II}), attributed to two distinct muonium centers (Mu^I and Mu^{II}), are observed at low temperature, whereas in CuI only a single pair of frequencies is observed. The frequencies were independent of crystal orientation, indicating that the hf interaction for these centers is isotropic. The reduced hf parameters ($A_r=A/A^{vac}$), determined from Eq. (4a) and extrapolated to 0 K, range between 0.2716 and 0.3744 (see Table I). Also included in Table I are ratios of g_e/g_μ determined from Eq. (4b). In all cases

TABLE I. Debye model parameters describing the temperature dependence of the reduced hyperfine parameter ($A_r=A/A^{vac}$) of Mu^I and Mu^{II} [see Eq. (16)]. The ratio between the electron and muon g factors for Mu^I at 5 K and Mu^{II} at 150 K are also included.

Center	$A_r(0)$	g_e/g_μ	κ	Θ_e (K)
Mu^I-CuCl	0.298 935(18)	1.0292(40)	−0.0858(6)	110(7)
Mu^{II}-CuCl	0.271 608(29)	1.0335(36)	−0.0796(5)	130(1)
Mu^I-CuBr	0.314 491(13)[a]	1.0207(15)		
Mu^{II}-CuBr	0.280 256(47)[a]	1.027(16)		
Mu^I-CuI	0.374 373(52)	1.0313(24)	+ 0.0080(2)	11.4(2)

[a]Extrapolated to $T=0$ with a modified Debye model in which Θ_e was allowed to vary above 100 K.

the observed g_e/g_μ is about 2–3% higher than for muonium in vacuum.

The temperature dependences of the Mu^I and Mu^{II} hf parameters in the Cu halides (see Fig. 4) were fitted to a Debye model,[23–25] in which it is assumed that the temperature variation in the hf parameter is due to muonium interaction with a Debye spectrum of acoustic phonons. This leads to the following functional form,

$$A_r(T)=A_r(0)\left[1-\kappa(T/\Theta_e)^4\int_0^{\theta_e/T}\frac{x^3}{e^x-1}\,dx\right], \qquad (16)$$

where Θ_e is the effective Debye temperature, $A_r(0)$ is the reduced hf parameter at 0 K, and κ is the coupling constant. The fit results for CuCl and CuI are given in Table I and shown in Fig. 4 (solid lines). In the case of CuBr, Eq. (16) does not fit the data because of the downward curvature above 100 K. The dashed curves in Fig. 4 for CuBr were obtained by allowing Θ_e to vary above 100 K and are only intended to guide the eye.

The temperature variation in the hf parameters in the Cu halides are unusual in several respects. First, in CuCl and CuBr the hf parameters increase monotonically with temperature—opposite of what is observed for most normal muonium defect centers. Second, the effective Debye temperature for the Mu^I center in CuI is an order of magnitude too small when compared with the literature value of the Debye temperature determined from specific-heat measurements.[26] Third, in CuBr the Debye model [Eq. (16)] fails to describe the high-temperature behavior of the Mu^I and Mu^{II} hf parameters. These facts suggest that lattice expansion, anharmonic effects, or details of the acoustic-phonon spectrum may be more important in the Cu halides than in other materials. Although a hydrostatic pressure experiment[23] indicates that thermal expansion has no appreciable effect on the Mu hf parameter in Si, it should be noted that the linear coefficients for thermal expansion in the Cu halides[27] are 4–6 times larger than in Si (Ref. 28) and increase from CuCl to CuBr to CuI. Also, the Cu halides are noted for their anharmonic vibrational properties.[29,30]

In the case of CuCl the Debye model fits the data and gives a reasonable value for Θ_e, equal to 110(7) K for Mu^I and 130(1) K for Mu^{II}. For comparison, the Debye temperature (Θ_D) in CuCl derived from specific-heat data[26] varies considerably over the temperature range of interest. At $T=0$ K, Θ_D equals 164 K, passes through a minimum at $T=10$ K where Θ_D equals 123 K, and rises to a maximum at $T=100$ K where Θ_D equals 260 K. Our effective Debye temperature should be compared with Θ_D at low temperature where the primary contribution to the heat capacity is from acoustic phonons. Considering the unusual thermal properties of the Cu halides, this apparent success of the model in CuCl is perhaps more surprising than its failure in CuBr and CuI.

B. The transition from Mu^I to Mu^{II}

The temperature dependence of the Mu^I and Mu^{II} precession amplitudes and exponential depolarization rates are shown on the left- and right-hand sides of Fig. 5, respectively. The total precession amplitudes are corrected for finite timing resolution and normalized to the maximum experimental asymmetry (the free-muon precession amplitude in Cu), after taking into account a small fraction of the muons which stop in the cryostat (~10%).

Below about 100 K the amplitudes for both Mu^I and

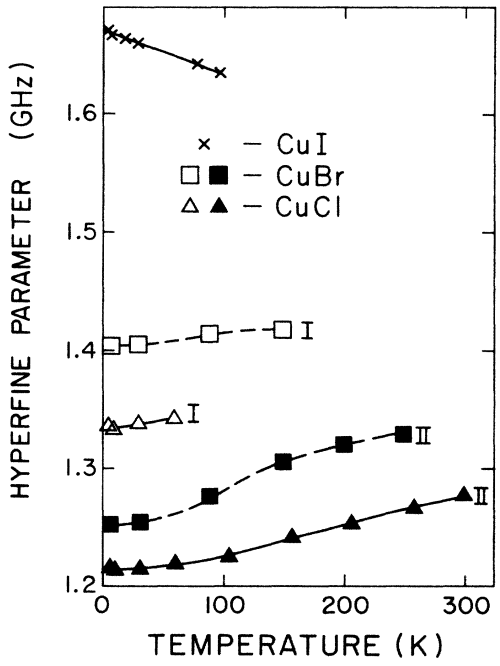

FIG. 4. The hyperfine parameters for muonium in the Cu halides as a function of temperature. In CuCl and CuBr two centers, Mu^I and Mu^{II} are observed, whereas in CuI only a single center is observed. The solid lines are a fit to a Debye model of the muonium phonon interaction. The dashed lines for CuBr are a guide to the eye.

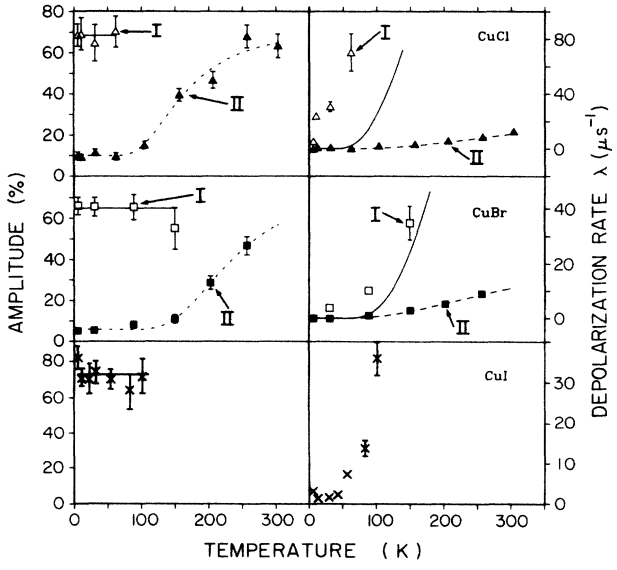

FIG. 5. The temperature dependence of the precession amplitudes (left) and depolarization rates (right) of the muonium centers observed in the Cu halides. The open and solid data points are for Mu^I and Mu^{II}, respectively.

Mu^{II} are independent of temperature. However, at higher temperatures the amplitude for Mu^{II}, which is observed only in CuCl and CuBr, increases monotonically and approaches the total precession amplitude observed at low temperature for both centers. The Mu^{I} center is not observable at the higher tempertures due to a sharp increase in the depolarization rate, although the amplitude of the signal remains constant. These facts indicate that Mu^{I} makes a thermally activated transition to Mu^{II}. The CuCl and CuBr data were therefore interpreted in terms of the transition model described in Sec. II D. The dashed lines on the left-hand side of Fig. 5 are fits to Eq. (11a) assuming an Arrhenius form for the transition rate [Eq. (12)]. The slight temperature dependence in ν_1 and ν_2 was taken into account using the fitted Debye model parameters. Since the amplitude of Mu^{II} is nonzero at low temperature, it was necessary to allow for a prompt fraction of muons (f_p^{II}) which form Mu^{II} at time zero in addition to a slow fraction (f_s^{II}) which begin as Mu^{I}. The fitted parameters defined as in Eqs. (11a) and (12) are found in Table II. The Mu^{I} fraction (f^{I}) observed at low temperature and the bare muon fraction (f_μ) are also included in Table II.

The dramatic difference in the temperature dependence of the depolarization rates for Mu^{I} and Mu^{II} in CuCl and CuBr (solid triangles and squares on the right-hand side of Fig. 5) support the hypothesis of a transition between Mu^{I} and Mu^{II} (see Sec. II D). The depolarization rate of the Mu^{II} center increases gradually with temperature and was described well by an Arrhenius law with a temperature-independent background term:

$$\lambda^{II}(T)=\lambda(\infty)\exp(-E_d/k_BT)+\lambda(0)\ . \tag{17}$$

The fitted parameters are found in Table III. There are several possible origins of this depolarization. The Mu^{II} center itself might be unstable to a transition to a diamagnetic muon center, which is observed to be the most stable state in Ge at high temperature.[31] Raman processes and Korringa relaxation are other possible mechanisms which have been proposed to explain relaxation of muonium at high temperature in other semiconductors.[32] The temperature dependence of the Mu^{I} depolarization rate is substantially different (open triangles and squares on the right-hand side of Fig. 5). The data do not fit well to a simple exponential. This is most evident in the case of CuCl where there is a sharp increase between 5 and 10 K.

TABLE II. Model parameters describing the thermally activated transition from Mu^{I} to Mu^{II} (see Sec. II D). The fitted parameters f_s^{II}, f_p^{II}, $\Lambda(\infty)$, and E_a/k are defined as in Eqs. (11a) and (12). The measured Mu^{I} amplitude (f^{I}) and the fraction of muons precessing as bare muons (f_μ) are also included.

	CuCl	CuBr	CuI
f_s^{II} (%)	66(3)	66(5)	
f_p^{II} (%)	9.9(8)	5.8(8)	
$\Lambda(\infty)$ (μs^{-1})	1330(100)	1195(107)	
E_a/k_B (K)	383(12)	582(18)	
f^{I} (%)	69(4)	65(3)	72(3)
f_μ (%)	16(4)	23(4)	18(8)

TABLE III. Parameters describing the Arrhenius temperature dependence of the depolarization rate of the Mu^{II} center in CuCl and CuBr [see Eq. (17)].

Sample	$\lambda(0)$ (μs^{-1})	$\lambda(\infty)$ (μs^{-1})	E_d/k_B (K)
CuCl	0.14(13)	60(12)	520(43)
CuBr	0.1(3.5)	48(22)	443(110)

It is important to note that $\lambda^{I}(T)$ increases in the temperature region immediately before the amplitude on the Mu^{II} center begins to rise. This is predicted from the transition model described in Sec. II D. The solid lines on the right-hand side of Fig. 5 are the predicted disappearance rate of Mu^{I} based on the rise of the Mu^{II} signal amplitudes. Note that the observed values for $\lambda^{I}(T)$ lie above the predicted curves, especially in the case of CuCl. A similar discrepancy has been reported for the Mu-to-Mu* transition observed in diamond[1] and was attributed to some additional relaxation process which affects Mu but not Mu*. Such an explanation seems unlikely in the present case since the Mu^{I} and Mu^{II} are so similar. Another possibility is that the transition itself is more complicated than we have allowed for. For example, the anomalous relaxation of Mu^{I} signal could be explained if there is an intermediate state between Mu^{I} and Mu^{II} or if there is some slow modulation of the Mu^{I} hf interaction prior to the transition. It is interesting to note that the preexponential factors $\Lambda(\infty)$ are quite small (see Table II), indicating that low-frequency acoustic vibrations control the transition.

The transition model parameters for CuCl and CuBr are compared in Table II. Note that in CuBr the initial occupation probability for Mu^{II} (f_p^{II}) is smaller and that the activation energy (E_a/k_B) for the transition is larger. If this is a trend which continues to the case of CuI, then this might explain the nonobservance of Mu^{II} in CuI. It suggests that the Mu^{II} center in CuI might be observed at higher temperatures.

C. Line broadening due to nuclear hyperfine interaction

Since all nuclei in the Cu halides have spin $\frac{3}{2}$ except for ^{127}I (100% abundant and spin $\frac{5}{2}$), one expects line broadening due to nhf interaction in low magnetic fields. As explained in Sec. II C, the field dependence of the linewidths provides information on the strength of the nhf interaction and on the mobility of the defect center. Significantly better fits to the μSR spectra taken at low magnetic fields were obtained assuming a Gaussian relaxation function for the Mu^{I} depolarization rates at low temperature, indicating that Mu^{I} is not moving rapidly. In the case of Mu^{II} the signals are too weak to distinguish between Gaussian and exponential depolarization functions. The static behavior of the Mu^{I} center is substantiated from the field dependence of the measured linewidth parameters determined from fits to Eq. (15b) and shown in Fig. 6. The solid curves are fits to the functional form

$$\sigma=\Delta\sin^2\theta+\sigma(\infty)\ , \tag{18}$$

TABLE IV. Parameters obtained by fitting the field dependence of the Gaussian line width parameter of muonium in the Cu halides to Eq. (18). An approximate nuclear hyperfine parameter, C, is obtained from Δ [defined in Eq. (7b)] by assuming that the muonium center interacts isotropically with four identical spin-$\frac{3}{2}$ nuclei, yielding $\Delta=\pi\sqrt{10}C$. The parameter $\sigma(\infty)$ is a field-independent background term.

Center	T (K)	Δ (μs^{-1})	$\sigma(\infty)$ (μs^{-1})	C (MHz)
Mu^{I}-CuCl	10.5	10035(970)	12.3(8)	1010(98)
Mu^{II}-CuCl	10.5	929(129)	0.0(3.5)	94(13)
Mu^{I}-CuBr	5.5	2002(70)	0.24(7)	202(7)
Mu^{II}-CuBr	5.5	1675(338)	0.80(54)	169(34)
Mu^{I}-CuI	10.5	2767(71)	0.72(10)	279(7)

where Δ and θ are defined as in Eq. (7a) and $\sigma(\infty)$ is a field-independent background term. Equation (18) is valid if the Mu centers are static or moving slowly with respect to the static linewidth. The fitted parameters are given in Table IV. An effective nhf parameter assuming four nearest-neighbor spin-$\frac{3}{2}$ nuclei is also included. In the case of Mu^{I} a much inferior fit to the data was obtained using Eq. (8) with a field-independent term. This is valid when the centers are moving rapidly. For example, the dashed curve in the bottom left of Fig. 6 is a fit to the fast-diffusion model in CuI. Due to the small amplitudes of the Mu^{II} center, it was not possible to distinguish fast diffusion from the static limit, although the magnitude of the linewidth itself suggests that no significant motional narrowing takes place.

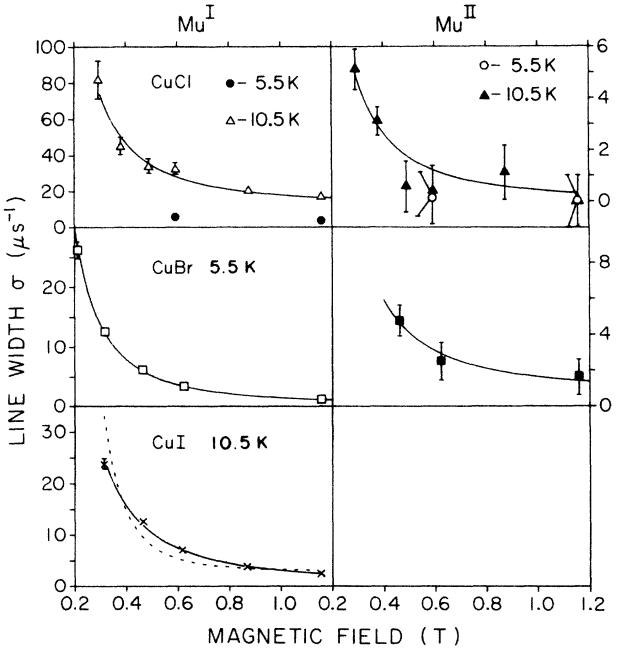

FIG. 6. The Gaussian relaxation parameter σ as a function of magnetic field for Mu^{I} (left) and Mu^{II} (right) in the Cu halides. The solid curves are fits to a static model [see Eq. (18)]. The dashed line in CuI is a fit to Eq. (8) with a field-independent background term, which is valid in the limit of fast diffusion. Mu^{II} was not observed in CuI.

With the exception of the Mu^{I} center in CuCl at 10.5 K, the effective nhf parameters in Table IV are of the order of a few hundred MHz. This compares well with the nhf parameters measured for other types of paramagnetic defect centers in the Cu halides such as CuCl:S and CuCl:Se.[33] However, in the case of Mu^{I} in CuCl at 10.5 K the field dependence of the line broadening indicates the nhf parameter is about 5 times that measured in CuBr and CuI, which seems unreasonably large. Interestingly, the two data points at a lower temperature of 5.5 K lie considerably below the points at 10.5 K (see top left of Fig. 6) and are consistent with a nhf parameter of a few hundred MHz or less. The muon hf parameter, on the other hand, shows no such dramatic change in this temperature region, indicating a smooth dependence of the electron-spin density on temperature. This puzzling behavior of the line broadening in CuCl is not understood.

V. DISCUSSION

A. Site possibilities for Mu^{I} and Mu^{II}

It is useful to summarize the relevant experimental information contained in the preceding section before discussing the site possibilities for the observed centers:

(1) In CuCl and CuBr we have observed two distinct muonium defect centers, Mu^{I} and Mu^{II}, which have nearly identical isotropic hf parameters, approximately 30% of the value for muonium in vacuum.

(2) The Mu^{I} center forms with a high probability at low temperatures but appears to be unstable, making a thermally activated transition to Mu^{II}.

(3) The line broadening at low magnetic fields, presumably due to nhf interaction, indicates that the observed centers are not moving rapidly.

We will show that these facts together indicate that the observed centers are most likely located at either one or both of the inequivalent tetrahedral interstitial sites.

The isotropic hf interaction implies that the electron and muon-spin densities are centered about a site with high symmetry or the center is moving rapidly between sites with lower symmetry (e.g., a site involving a native impurity) in a way which averages out the anisotropy.

Since there appears to be no motional averaging of the nhf interaction, this virtually rules out the latter possibility. In the zinc-blende crystal structure there are only four high-symmetry sites—the two substitutional sites and the two tetrahedral interstitial sites.

There are several arguments against assigning Mu^I and Mu^{II} to the two different substutional sites. The hf parameters for Mu^I and Mu^{II} are quite small, indicating there is substantial covalent bonding to the nearest neighbors. Thus the hf parameters are expected to be quite sensitive to the type of nearest neighbors. Since the two substitutional sites are extremely dissimilar, having four Cu (halide) nearest neighbors and 12 halide (Cu) next-nearest neighbors 1.63 times more distant, one would expect the hf parameters for the two substitutional Mu centers to be quite different. In contrast with this, the observed hf parameters for Mu^I and Mu^{II} differ by only 3% in both CuCl and CuBr (see Table I). In addition, we can find no reasonable explanation for the observed transition from Mu^I to Mu^{II} since it would necessarily involve the appearance of a Cu (halide) atom and the disappearance of a halide (Cu) atom.

One may overcome these difficulties if Mu^I and Mu^{II} are located at the same substitutional site, implying that Mu^I is a metastable excited state of Mu^{II}. However, the observed centers form with a relatively high probability ($\sim 70\%$) with no other paramagnetic center being formed. In order to be observed in a muon precession experiment the center must be formed in a time much less than the precession period (~ 2 ns). An unreasonably large vacancy concentration and muonium mobility would be necessary to account for such rapid formation. Alternatively, substitutional muonium centers might form epithermally via a knockout reaction or by trapping immediately after thermalization at a vacancy created by the muon. In this case one would expect a considerable probability for other types of centers to be formed, such as the interstitial center. However, it is clear from Table II that the observed centers account for almost all the muon polarization.

The arguments against one center being substutional and one center being interstitial are similar to those made against the two substitutional sites. A tetrahedral interstitial site has four nearest neighbors of one type and six next-nearest neighbors of the opposite type, 1.15 times more distant. This is considerably different than the substitutional site described above. Thus it is doubtful that such dissimilar environments would lead to nearly identical hf parameters. Note also that the Mu^I center is not moving rapidly and that neither center can be sitting next to an interstitial atom or a vacancy since this would give rise to an anisotropic muon hf interaction. Considering these points, the observed transition from Mu^I to Mu^{II} is difficult to explain with this site assignment.

The two tetrahedral interstitial sites are the most reasonable site assignment for Mu^I and Mu^{II}. The normal muonium center in the elemental semiconductors is believed to be diffusing rapidly between equivalent tetrahedral interstitial sites. In a compound semiconductor one might expect to observe two such centers since there are two inequivalent tetrahedral interstitial sites. This would imply that the Mu^I and Mu^{II} are static since equivalent tetrahedral sites are separated by an inequivalent site. This is consistent with the linewidth measurements in Sec. IV C. It is also reasonable that one center be less stable than the other and that there be a thermally activated transition from one site to the other. Moreover, one might argue that the similarity in the muon hf parameters for Mu^I and Mu^{II} is reasonable since the two inequivalent tetrahedral sites are quite similar. The next-nearest-neighbor nuclei of one type are only 1.15 times more distant from the muon than the four nearest neighbors of the other type. Lattice distortion might tend to further equalize the two environments. Even considering this, the near equality of the hf parameters for Mu^I and Mu^{II} is remarkable. We have no explanation for why the less stable center, Mu^I, is populated preferentially.

The only remaining site possibility is that Mu^I and Mu^{II} correspond to the same interstitial tetrahedral site, implying that Mu^I is an excited state of Mu^{II}. Mu^I cannot be an *electronically* excited state of Mu^{II} since the hf parameters for the two centers are so close. Also, a vibrational excited state of muonium seems unlikely to have a lifetime in the order of microseconds. If Mu^I is an excited state of Mu^{II}, then the nature of the excitation is probably connected with the distortion of the lattice around the muon. This excited-state model would nicely explain the close similarity in the hf parameters for Mu^I and Mu^{II} and the observed thermally activated transition from one center to the other. However, the suggestion that two highly symmetric lattice-distortion modes around the muon are both stable on a timescale of microseconds is questionable considering there is no evidence for such a phenomenon in other tetrahedrally coordinated materials. On the other hand, it should be noted that the cuprous halides have an ionicity close to the critical value which separates tetrahedral from octahedral coordination. Consequently, they display a number of peculiar properties such as a complex phase diagram,[34] large thermal-expansion coefficients,[27,28] and abnormally small bulk moduli.[35]

B. The small hyperfine parameters for Mu^I and Mu^{II}

The hf parameters for Mu^I and Mu^{II} in the cuprous halides are unusually small when compared to the Mu centers with isotropic hf parameters that have been observed in other semiconductors and insulators. The reduction in the hf interaction for muonium centers may be considered a covalency effect: The unpaired-electron wave function is a covalent mixture of the muonium $1s$ wave function and the surrounding host orbitals. This lowers the spin density on the muon and reduces the hf interaction. One might expect this local covalency to be correlated with the covalency or ionicity of the host. In Fig. 7 the reduced hf parameters in various semiconductors and insulators are plotted as a function of the Philips ionicity,[36] $f_i = 1 - f_c$, where f_c is the covalency. In general, there appears to be a positive correlation between the muon hf parameter and ionicity. A nonlinear behavior might be expected in materials composed of elements belonging to different rows of the Periodic Table since the

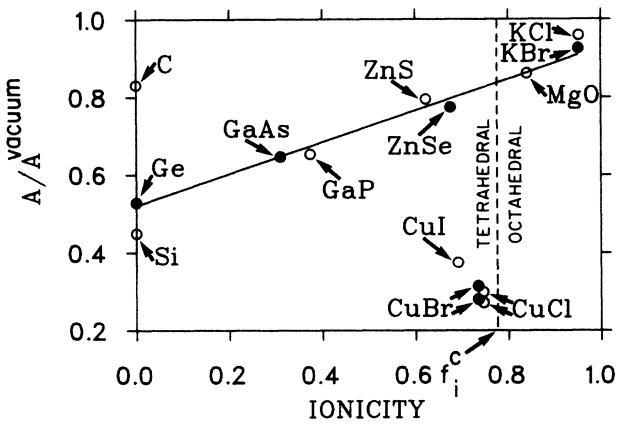

FIG. 7. The reduced hyperfine parameter for muonium in semiconductors and insulators as a function of the Philips ionicity. Compounds to the left of the critical ionicity ($f_i^c=0.785$) are tetrahedrally coordinated, whereas those to the right are octahedrally coordinated. The solid data points are for compounds (elements) lying on the same row of the Periodic Table. The data for the elemental semiconductors are from Ref. 1, the group—III-V materials from Ref. 7, KCl from Ref. 6. The reduced hyperfine parameters for ZnSe at 13 K, ZnS at 10 K, MgO at 300 K, and KBr at 232 K are 0.774 05(8), 0.794 89(8), 0.862 46(6), and 0.924 58(4), respectively, from the present work.

hf interaction is most likely correlated with other parameters as well, such as the lattice constant and the type of valence orbitals. This is most evident in the case of pure covalent materials, diamond, Si, and Ge, where there is significant variation in A_r. One might also expect a discontinuity at the critical ionicity ($f_i^c=0.785$), where the coordination changes from tetrahedral to octahedral. However, if one compares materials on the same row such as Ge, GaAs, ZnSe, and KBr, one finds a near perfect linear relationship between f_i and A_r, even though KBr has rocksalt structure whereas all of the others have zinc-blende crystal structure. The hf parameters observed in the Cu halides are thus anomalously small when compared with the other materials. The case of CuBr is particularly interesting since it is composed of elements on the same row as Ge, GaAs, ZnSe, and KBr. Thus the bonding characteristics of muonium appear to be substantially different in the Cu halides compared with the other materials.

The reasons for this anomalous behavior are not clear, but it should be noted that the Cu halides have a number of unusual electrical and lattice-vibrational properties which may be related to the present observations. For example, it has been reported that the uppermost valence band consists principally of Cu $3d$ states and not sp^3 hybrid states as in the other tetrahedrally coordinated semiconductors.[37] Detailed electronic-structure calculations might reveal whether the peculiarity in band structure of the Cu halides is related to the small hf parameters for Mu^I and Mu^{II}. The Cu halides have an ionicity close to the critical ionicity and therefore are on the limit of stability. This is believed to be responsible for many of the unusual properties of the Cu halides, which include abnormally small bulk and shear moduli,[35] rather complex phase diagrams,[34] and enhanced anharmonic lattice vibrations.[29,30] Thus, lattice distortion and lattice vibration may play a prominent role in determining the muonium hf parameters in the Cu halides.

Finally, considering the size of the anomaly in the Cu halides one should also examine the possibility that the observed centers in the Cu halides are somehow electronically inequivalent to the normal muonium centers observed in the other materials. For example, in the Cu halides the muonium defect centers (including the neighboring atoms) might have an overall charge of $+2$, rather than being neutral. This would certainly alter the bonding characteristics dramatically. However, it is difficult to understand why the neutral defect is not formed with some significant probability. Another possibility is that the observed centers are the analogue of the Mu^* center observed in the group-IV and III-V semiconductors, which has a small anisotropic hf interaction with $\langle 111 \rangle$ symmetry. It is possible that the corresponding center in the group—I-VII semiconductors has an isotropic hf interaction. There is still considerable debate on the site of Mu^*. However, recent calculations[13–15] favor a substitutional site. This is not consistent with our interpretation of the present experimental results that the observed centers in the Cu halides are interstitial.

VI. SUMMARY AND CONCLUSION

We have reported detailed measurements on the hyperfine structure of muonium defect centers in the group—I-VII semiconductors CuCl, CuBr, and CuI. The centers appear to be similar to the normal muonium observed in other tetrahedrally coordinated semiconductors in that they are characterized by isotropic hyperfine interactions which are reduced in strength from the vacuum value by a factor of about 2–3. Symmetry arguments suggest that the centers are located at a tetrahedral interstitial site, as is believed to be the case for normal muonium. However, there are also peculiarities which distinguish the centers observed in the Cu halides from those in other tetrahedrally coordinated materials. First, in CuCl and CuBr two distinct centers with almost identical isotropic hyperfine parameters are observed. Although in the group-IV and group—III-V materials two centers are also observed (normal and anomalous muonium), the hyperfine interaction for anomalous muonium is much smaller than for normal muonium, and, moreover, it is anisotropic. Second, if one plots the hyperfine parameters of muonium in a variety of semiconductors and insulators versus their ionicity, one finds that muonium centers in the Cu halides have abnormally small hyperfine parameters. This indicates that the covalent bonding of muonium in these materials is quite unusual. It is not clear whether this is because (1) there is a peculiarity in the host electronic structure, (2) the ionicity of the Cu halides is close to the critical value which separates tetrahedral from octahedral coordination, or (3) muonium in the Cu halides is somehow electronically inequivalent to the normal muonium seen in other materials.

We have also observed in interesting dynamical

phenomenon in CuCl and CuBr—the Mu^I center which is populated preferentially at low temperature makes a thermally activated transition to Mu^{II} at higher temperatures. We find that the most reasonable site assignment is that Mu^I and Mu^{II} are located at the two inequivalent tetrahedral interstitial sites, respectively, although we cannot dismiss other more exotic possibilities such as that Mu^I is a metastable excited state of Mu^{II} located at a single tetrahedral interstitial site.

ACKNOWLEDGMENTS

This work was supported by the Swiss National Science Foundation and by the U.S. National Science Foundation through Grant No. DMR-79-09223. We would also like to thank the Swiss Institute of Nuclear Research for their cooperation and especially David George of the Magnet Group for this design of the special low-fringe field magnet.

*Present address: TRIUMF, Vancouver, B.C., V6T 2A3 Canada.

[1]E. Holzschuh, W. Kündig, P. F. Meier, B. D. Patterson, J. P. Sellshop, M. C. Stemmet, and H. Appel, Phys. Rev. A **25**, 1272 (1982).

[2]K. W. Blazey, T. L. Estle, E. Holzschuh, W. Odermatt, and B. D. Patterson, Phys. Rev. B **27**, 15 (1983).

[3]R. F. Kiefl, J. B. Warren, G. M. Marshall, C. J. Oram, and C. W. Clawson, J. Chem. Phys. **74**, 308 (1981).

[4]J. H. Brewer, D. S. Beder, and D. P. Spencer, Phys. Rev. Lett. **42**, 808 (1981).

[5]P. W. Percival, K. M. Adamson-Sharpe, J. C. Brodovitch, Siu-Keung Leung, and K. E. Newman, Chem. Phys. **95**, 321 (1985).

[6]R. F. Kiefl, E. Holzschuh, H. Keller, W. Kündig, P. F. Meier, B. D. Patterson, J. W. Schneider, K. W. Blazey, S. L. Rudaz, and A. B. Denison, Phys. Rev. Lett. **53**, 90 (1984).

[7]R. F. Kiefl, J. W. Schneider, H. Keller, W. Kündig, W. Odermatt, B. D. Patterson, K. W. Blazey, T. L. Estle, and S. L. Rudaz, Phys. Rev. B **32**, 530 (1985).

[8]N. Sahoo, S. K. Mishra, K. C. Mishra, A. Coker, T. P. Das, C. K. Mitra, and L. C. Snyder, Phys. Rev. Lett. **50**, 913 (1983).

[9]A. Mainwood and A. M. Stoneham, Physica **116B**, 101 (1983).

[10]A. Mainwood and A. M. Stoneham, J. Phys. C **17**, 2513 (1984).

[11]H. Katayama-Yoshida and K. Shindo, J. Phys. Soc. Jpn. **53**, 1114 (1984).

[12]K. P. Döring, K. P. Arnold, M. Gladisch, N. Haas, E. E. Haller, D. Herlich, W. Jacobs, M. Krause, M. Krauth, H. Orth, and A. Seeger, Hyperfine Interact. **17-19**, 629 (1984).

[13]N. Sahoo, K. C. Mishra, and T. P. Das, Phys. Rev. Lett. **55**, 1506 (1985).

[14]A. Mainwood, T. L. Estle, and A. M. Stoneham (private communication).

[15]T. L. Estle, Hyperfine Interact. **17-19**, 585 (1984).

[16]T. L. Estle, Hyperfine Interact. **8**, 365 (1981), and references therein.

[17]K. W. Blazey, T. L. Estle, E. Holzschuh, P. F. Meier, B. D. Patterson, and M. Richner, Hyperfine Interact. **17-19**, 595 (1984).

[18]C. S. Wu and V. W. Hughes, in *Muon Physics,* edited by V. W. Hughes and C. S. Wu (Academic, New York, 1976), p. 85.

[19]E. Roduner and H. Fischer, Chem. Phys. **54**, 261 (1981).

[20]P. W. Precival and H. Fischer, Chem. Phys. **16**, 89 (1976).

[21]P. F. Meier, Phys. Rev. A **25**, 1287 (1982).

[22]C. Schwab and A. Goltzené, Prog. Cryst. Growth Charact. **5**, 233 (1982).

[23]E. Holzschuh, Phys. Rev. B **27**, 102 (1983).

[24]E. Simanek and R. Orbach, Phys. Rev. **145**, 191 (1966).

[25]S. G. Sligar and H. Blum, Phys. Rev. B **3**, 3587 (1971).

[26]Z. Vardeny, G. Gilat, and D. Moses, Phys. Rev. B **18**, 4487 (1978).

[27]Approximate values for the linear coefficient of thermal expansion in CuCl, CuBr, and CuI between 200 and 300 K are estimated to be 11×10^{-6}, 14×10^{-6}, and 16×10^{-6} K^{-1} using data from H. F. Schaake, Air Force Research laboratory Report No. AFCRL-69-0538, 1969 (unpublished).

[28]In Si at 250 K the linear coefficient of thermal expansion equals 2.1×10^{-6} K^{-1} [*American Institute of Physics Handbook,* 3rd ed. (McGraw-Hill, New York, 1972)].

[29]S. Hoshino, Y. Fujii, J. Harada, and J. D. Axe, J. Phys. Soc. Jpn. **41**, 965 (1976).

[30]J. Harada, H. Suzuki, and S. Hoshino, J. Phys. Soc. Jpn. **41**, 1707 (1976).

[31]V. I. Kundinov, E. V. Minaichev, G. G. Myasishcheva, Yu. V. Obukhov, V. S. Roganov, G. I. Savel'ev, V. M. Samoilov, and V. G. Firsov, Zh. Eksp. Teor. Fiz. **70**, 2041 (1976) [Sov. Phys.—JETP **43**, 1065 (1976)].

[32]A. Weidinger, G. Balzer, H. Graf, E. Recknagel, and Th. Wickert, Phys. Rev. B **24**, 6185 (1981).

[33]A. Goltzene, C. Schwab, B. Meyer, and S. Nikitine, Opt. Commun. **5**, 248 (1972).

[34]E. R. Rapoport and C. W. T. Pistorius, Phys. Rev. **172**, 838 (1968).

[35]R. M. Martin, Phys. Rev. B **1**, 4005 (1970).

[36]J. C. Philips, Rev. Mod. Phys. **42**, 317 (1970).

[37]A. Zunger and M. L. Cohen, Phys. Rev. B **20**, 1189 (1979); A. Goldman, Phys. Status Solidi B **81**, 9 (1977).